Real-time Detection of Acetaldehyde in Electrochemical CO Reduction on Cu Single Crystals

Yu Qiao, Degenhart Hochfilzer, Jakob Kibsgaard, Ib Chorkendorff, Brian Seger*

Author information

Corresponding Author

* Brian Seger– Surface Physics and Catalysis (SurfCat) Section, Department of Physics, Technical University of Denmark, 2800 Kgs. Lyngby, Denmark brse@fysik.dtu.dk

Authors

Yu Qiao – Surface Physics and Catalysis (SurfCat) Section, Department of Physics, Technical University of Denmark, 2800 Kgs. Lyngby, Denmark yuaqi@dtu.dk

Degenhart Hochfilzer – Surface Physics and Catalysis (SurfCat) Section, Department of Physics, Technical University of Denmark, 2800 Kgs. Lyngby, Denmark deho@dtu.dk

Jakob Kibsgaard – Surface Physics and Catalysis (SurfCat) Section, Department of Physics, Technical University of Denmark, 2800 Kgs. Lyngby, Denmark jkib@fysik.dtu.dk

Ib Chorkendorff – Surface Physics and Catalysis (SurfCat) Section, Department of Physics, Technical University of Denmark, 2800 Kgs. Lyngby, Denmark ibchork@fysik.dtu.dk

Abstract

Copper is known to be versatile in producing various products from electrochemical CO_2 reduction reaction (eCO2RR), and the product preference depends on reaction environments. Literature have reported alkaline electrolytes favor acetate production, and proposed hypotheses on the reaction pathway accordingly. Our work shows acetate can also come from the non-faradaic chemical oxidation of acetaldehyde in alkaline environments, which occurs quite rapidly compared to the typical measurement time interval. This adds uncertainties into both acetaldehyde and acetate production. With an electrochemistry-mass spectrometry combined (EC-MS) system, we present real-time detection of acetaldehyde as a function of applied potential on single crystal Cu electrodes during electrochemical CO reduction reaction (eCORR). In 0.1M KOH, the (100) and (211) facets had an acetaldehyde production onset of -0.35 V vs. RHE, whereas (111) and (110) exhibited no detectable acetaldehyde production up to -0.6 V vs. RHE. Moreover, the quantified acetaldehyde-to-ethylene production ratio provides insightful information on the acetaldehyde-to-ethylene bifurcation point in eCO2RR, and thus help understand the reaction pathways.

TOC Graphic

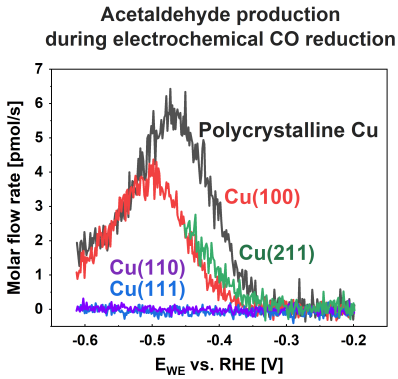

Electrochemical CO_2 reduction (eCO2RR) stores renewable energy in chemical bonds by converting CO_2 into chemicals and fuels. This strategy provides an avenue for closing the carbon balance and curtailing CO_2 emissions. Copper (Cu) is known to be the only monometallic metal that produces multiple hydrocarbons and oxygenates, and the product selectivity is dependent on the reaction environment. [1] As CO_2 forms buffering carbonates and bicarbonates with water, this limits the ability to modify the reaction environment. However, the first stable intermediate in CO_2 reduction on copper is well known to be CO. As CO does not form pH buffering species, electrochemical CO reduction (eCORR) can work as a CO_2 reduction proxy allowing us to vary pH. Using this approach, previous studies have reported that alkaline conditions favor producing acetate, and proposed hypotheses of the formation pathways of acetate production in eCORR [2–8]. Recent theoretical models along with experimental support suggested acetate formation via a non-faradaic homogenous reaction of a ketene-based entity [8].

In this letter, we demonstrate that instead of only being produced directly from eCO2RR, acetate can also be formed by non-faradaic chemical oxidation of acetaldehyde in alkaline solutions. Therefore, time delay in measuring the post-reaction electrolyte may lead to an overestimated productivity on acetate while underestimating acetaldehyde productivity, and thus mislead predictions on the formation pathways of both products. To eliminate the issue due to delayed acetaldehyde measurements, we performed real-time *operando* detection of acetaldehyde production on Cu electrodes during eCORR on an electrochemistry-mass spectrometry (EC-MS) system. The necessity, feasibility, and sensitivity of real-time acetaldehyde production detection were validated on polycrystalline Cu first, and then on single crystal Cu electrodes (Cu(hkl)). The presented potential- and facet-dependent acetaldehyde production as well as acetaldehyde *vs.* ethylene production bifurcation provides valuable mechanistic information on the yet-to-be-fully-understood eCORR pathways.

Why does acetaldehyde need to be measured as soon as possible? Previous studies suggest that acetaldehyde and ethanol are both products from eCORR/eCO2RR, and that ethanol comes from further reduction of acetaldehyde [9–11]. However, acetaldehyde is rarely included in the product distribution list, especially in eCORR conducted in alkaline conditions. This is mainly because acetaldehyde is unstable and undergoes complicated chemical conversions in alkaline solutions, such as Cannizzaro reaction, aldol reaction, Tishchenko reaction, self-condensation, and polymerization [4,12–14], making measurement of its concentration in post-mortem electrolytes challenging. To investigate the stability of acetaldehyde in alkaline solutions, ~5 mM acetaldehyde was added to 0.1 M KOH and the electrolyte composition was analyzed every hour for 10 hrs with high-performance liquid chromatography (HPLC). All major electrolyte

species (*i.e.*, concentration > 0.10 mM) are plotted in Figure 1a. There is a clear relationship between acetaldehyde decreasing and acetate increasing, indicating oxidation of acetaldehyde to acetate. While acetaldehyde oxidation to acetate can occur *via* the Cannizzaro reaction - a disproportionation of two acetaldehyde molecules to one acetate and one ethanol molecule [4,12,15], the lack of any ethanol entails this is not occurring substantially in our case. During the 24-hour test the electrolyte shifts from transparent to a yellow color (Figure s2), which might be indicative of self-polymerization of acetaldehyde in alkaline conditions [16,17]. Figure 1a also shows the alpha carbon of acetaldehyde can also be oxidized to form glycolaldehyde in small amounts. Given that small amounts of glycolaldehyde are sometimes seen in eCORR, the non-Faradaic oxidation of acetaldehyde with oxygen from water or the air, happening after the post-reaction sample is collected but before analysis, could be one explanation for this [18,19]. Taken together, these results show the complexities in accurately measuring acetaldehyde production from eCORR in alkaline conditions.

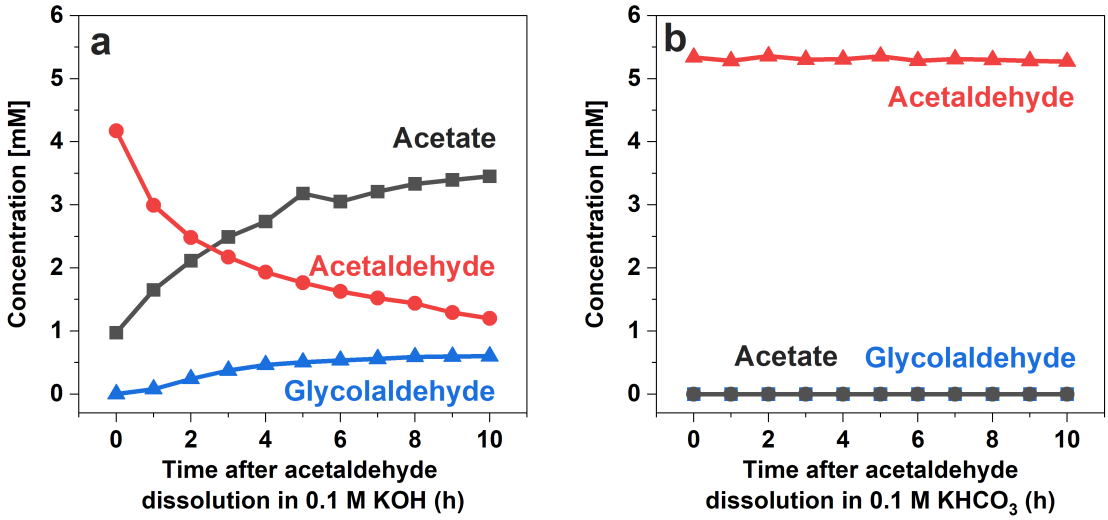

Figure 1. Composition change in the a) 5 mM Acetaldehyde – 0.1 M KOH and b) a) 5 mM Acetaldehyde – 0.1 M $KHCO_3$ mixture tracked during 10 hrs. Only composites with over 0.1 mM of concentration are shown. Other detected composites with < 1 mM concentration, as well as un-assigned HPLC chromatogram peaks, are plotted in Figure S1.

The presence of other components in addition to acetaldehyde at 0 h is due to time delay during the measurement: the HPLC sample was prepared *ca.* 10 min before injecting to the analyzing column, and the analysis took another ~30 min before the results could be acquired. This further demonstrates the fast conversion of acetaldehyde in alkaline and stresses the need for real-time detection in eCORR. In contrast, acetaldehyde degradation was not found to occur in an electrolyte of 0.1 M $KHCO_3$ (pH 6.8) over 10 hours (Figure 1b), which confirms the degradation is caused by the alkalinity of the electrolyte.

It should be noted that any industrially relevant CO electrolysis will need to operate at high current density. Since stoichiometrically CO reduction always produces OH^- along with products at the cathode, the result is that CO electrolysis will always occur in alkaline conditions at equilibrium. Previous work has shown that even if a pH buffering carbonate solution is used initially, the solution gets converted to an alkaline solution once equilibrium is reached (as the carbonate degasses as CO_2 at an acid-producing anode) [20].

Previous studies have shown that alkaline environment favor acetate production, and proposed some hypotheses on acetate reaction pathways accordingly [2–6,8,21]. However, it is possible that the promoted

acetate production observed in alkaline is at least partially due to the abovementioned alkaline-induced acetaldehyde oxidation. Therefore, analyzing liquid products in alkaline electrolytes immediately after the reaction is the best strategy to mitigate potential impacts from the alkalinity of the post-reaction electrolyte. Yet, in the case where immediate measurement is technically unfeasible, the authors suggest neutralizing the electrolyte before analysis to effectively keep acetaldehyde and acetate stable and thus improve the precision of liquid product measurement.

Real-time detection of acetaldehyde production in eCORR with EC-MS. As the most accurate way to measure acetaldehyde would be to measure it in real time, a device such as an electrochemical mass spectrometer (EC-MS) is perfectly suited for this need. Briefly, an EC-MS allows the removal of vapor products instantaneously and then directly transfers the vapor into a mass spectrometer (MS). This allows product analysis in the sub-seconds time scale. Therefore, an EC-MS enables us to resolve issues with acetaldehyde degradation due to the electrolytes' alkalinity. Further details regarding the working mechanism of the EC-MS have been published elsewhere [22].

One of the complexities of using MS with CO_2 or CO electrolysis is that multiple products are produced simultaneously, and they are ionized to fragments with identical m/z in the MS, making it challenging to differentiate different products. Specifically, the applied electron energy (EE) should not be so high that the target analyte molecules are severely fragmented and generate too many small fragments (*e.g.*, CH_2+, CH+, CO+, *etc.*) that are shared by most hydrocarbons and oxygenates while on the other hand, an excessively low EE would not effectively ionize the target molecules. Furthermore, since acetaldehyde and ethanol have similar molecular structures and thus similar ionized fragments, their differentiation requires optimizing the EE. Fortunately, the EC-MS we used allowed us to vary EE from 19 eV to 70 eV. This enables us to vary the degree of fragmentation of different products. The determined EE with the optimal sensitivity towards acetaldehyde and even ethanol was at 28 eV. The exact details of why 28 eV was used are described further in the supporting information.

Figure 2 plots the linear sweep voltammetry (LSV) scans and tracked m/z fragments of corresponding species as a function of the polycrystalline Cu working electrode potential (E_{WE}) during eCORR. The advantage of the EC-MS comes into play as evidenced by a highly time-resolved measurement (demonstrated in Figure S8) in ethylene production as shown in Figure 2c. In Figure 2b, methane production is also observed, though the low signal-to-noise ratio is indicative of the typical low methane selectivity for CO reduction in high pH electrolytes [2]. However, the most interesting peak is that of the acetaldehyde at M42 (Figure 2e). There is a sharp exponential increase starting at -0.35 V *vs.* RHE and decreases at more cathodic potentials starting at *ca.* -0.48 V *vs.* RHE. This could suggest that the acetaldehyde decrease is due to a further conversion to ethanol. As ethanol has a much lower vapor pressure than acetaldehyde at 25 °C (0.07 bar *vs.* 1.07 bar [23]), the sensitivity of ethanol in the MS is relatively low. From Figure S7, the increment in M31 is so low that it is within the noise or possibly related to other factors. Furthermore, at such low signals, the $C^{12}O^{18}$ isotopes (originating from the carrier gas CO) could be chemically ionized by H_2+ (coming from HER), leading to a M31 signal being detected. Thus, on this basis, our analysis is limited to only acetaldehyde for *in situ* liquid product analysis. With the demonstrated real-time detection of acetaldehyde on the EC-MS system, the next section is on the mechanistic studies on eCORR on single crystal Cu electrodes. Calibration of acetaldehyde and other products including hydrogen, methane and ethylene are also carried out and presented in detail in SI-S3. All further figures are presented in terms of mols rather than MS signal.

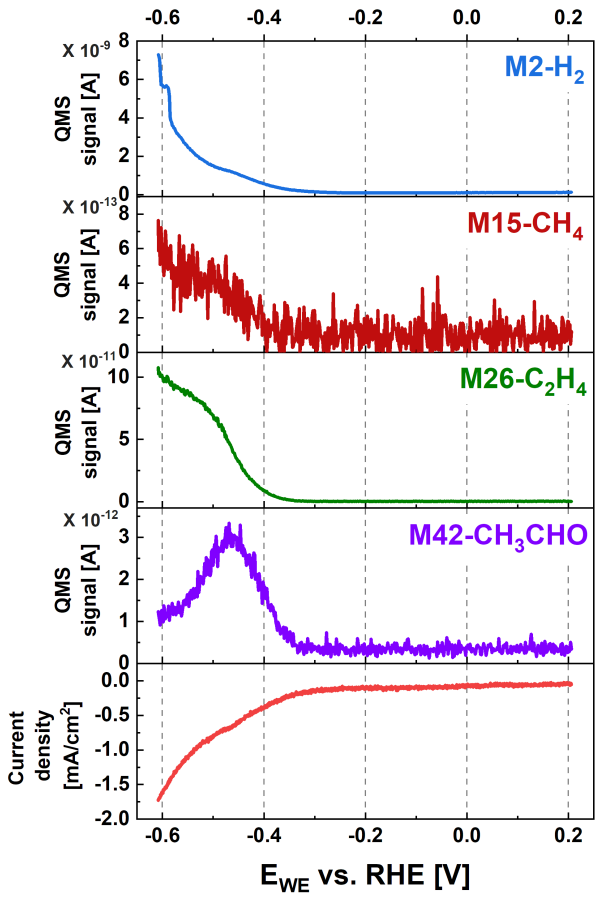

Figure 2. Linear sweep voltammetry scans and deconvoluted MS signals of electrochemical CO reduction on a polycrystalline Cu electrode in 0.1 M KOH. The scan rate was 2 mV/s to keep the system at a pseudo-steady state. Initially, the Cu electrode was kept at 0.2 V for 5min to reduce oxidized Cu on the surface to its metallic state, then started LSV scan from 0.2 V without going back to OCV. The same scales are used for the same m/z and electrochemistry data on the two metals.

Facet-dependent production distribution on Cu in eCORR. CO electrolysis was subsequently conducted in 0.1 M KOH on four Cu single crystal electrodes: (100), (110), (111), (211), and compared with the polycrystalline results, as shown in Figure 3.

Noticeably, the total current density at 0 V *vs*. RHE on Cu (110) and Cu (211) was relatively high (Figure 3e). This current was well reproducible over multiple tests on each facet. Since each Cu electrode was reduced at 0 V *vs*. RHE for 5 min before eCORR started, the reduction of oxidized Cu should not be the reason. On the other hand, oxygen reduction reaction (ORR) is a possible explanation. Considering the cell configuration (Figure S13), there could be a very small amount of air dissolved in the electrolyte, and that ORR was operating with a 0.77 V overpotential at 0 V *vs.* RHE [24], it is very likely to be mass transfer limited. However, since the consumption of O_2 was so low that it was below the detection limit, the change in M32 (descriptor for O_2) signal intensity was not observed. Moreover, as OH^- is produced from ORR, the (local) pH would increase which might also influence the current density, However, there was no literature that could be found explaining the facet or pH dependence of ORR on metallic Cu electrodes in alkaline environments, thus we cannot draw a full conclusion on the unexpected current. Nevertheless, the main argument regarding facet-dependent product preference is not influenced. More analysis regarding this can be found in SI-S4.4.

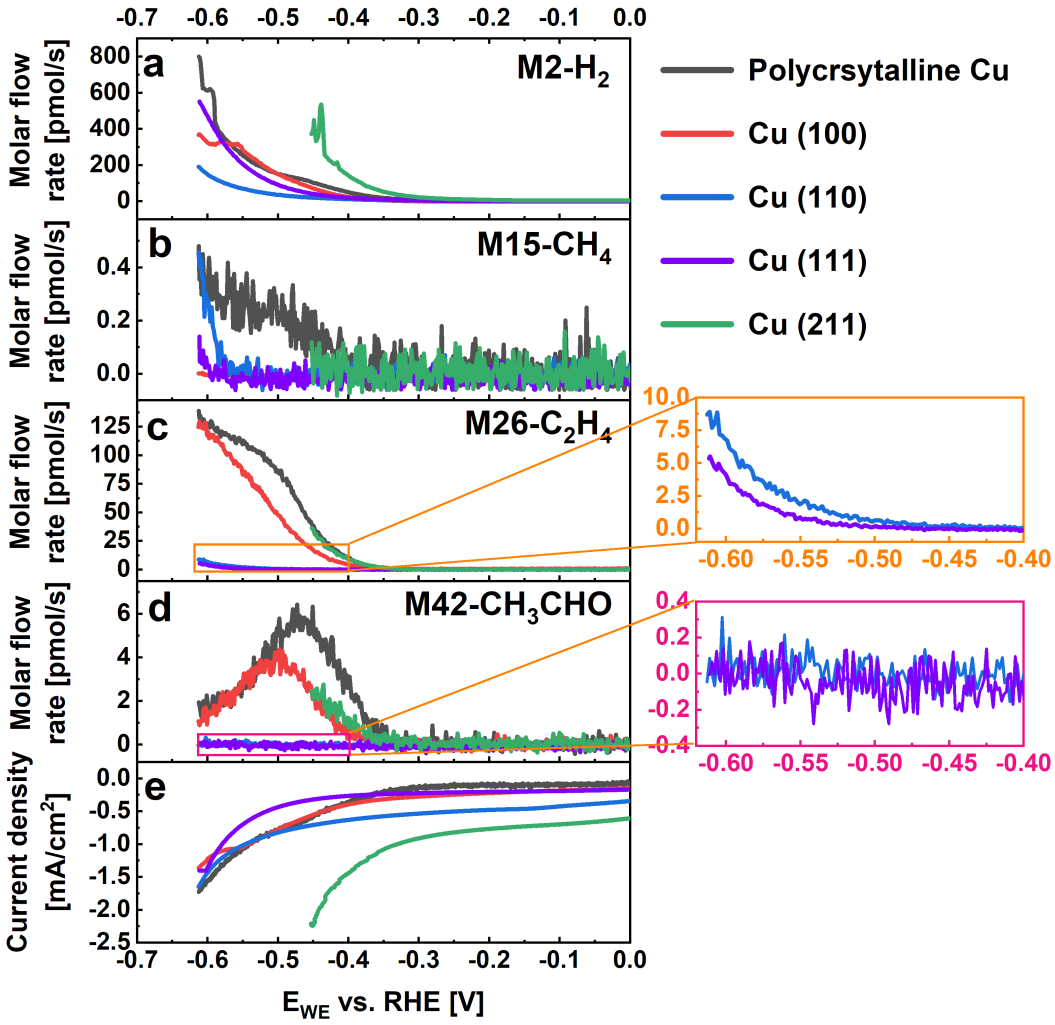

Figure 3. Electrochemical CO reduction performance comparison among polycrystalline Cu and single crystals in 0.1 M KOH. LSV scans start from 0 V vs. RHE until the potentiostat is overloaded, at the scan rate of 2 mV/s. The working electrode was kept at 0 V vs. RHE for 5 min to reduce oxidized Cu to its metallic state, then continued with an LSV without going back to OCV. All MS signals are converted to the molar flow rate (a-d) of the corresponding species. Magnified regions of panels c and d in the boxes are shown to the right. In panel c (M26-C_2H_4), (211) (green) and pc (black) overlapped.

In terms of eCORR performance, both the (111) and (110) facets exhibit higher onset overpotential and lower activity of all detected products compared to the polycrystalline Cu. For both these facets ethylene (Figure 3c) is the dominant eCORR product yet occurs at a *ca.* 200 mV higher overpotential than the polycrystalline Cu. For CH_4 (Figure 3b), the (111) and (110) also have similar onset potentials with the (110) being slightly more active. Previous Raman and DFT studies have found that (110) binds *CO the strongest among the three low-index facets [25,26] [27], and that *CO dimerization is more favorable on the square sites on the Cu(100) geometry [28–30], *CO protonation to CH_4 is preferred on Cu(110). This helps explain the higher CH_4 activity on (110) compared to the (111) facet.

Acetaldehyde was not found on (111) or (110) facets (Figure 3d). This is most likely to be either because acetaldehyde was not produced or the produced amount was below the detection limit, again which we can attribute to the low activity of *CO dimerization[31–34]. It should be noted that the lack of acetaldehyde is in contrast to the work of Hori on Cu(110), where substantial amounts of acetaldehyde were observed.

[31,35–37]. However, the difference may be attributed to that Hori used a more neutral pH and operated at 850 mV higher overpotential. It may also be that not only the produced amount was minimal, but acetaldehyde's further reduction to ethanol was so fast that acetaldehyde has been consumed already before being detected. Comparing product preference on the three low-index Cu facets (*i.e.* (111), (100), and (110)), ethylene is the most favored on (100), which is in line with most previous Cu (hkl) studies both experimentally [31,38,39] and theoretically [34,40,41]. Unlike many other single crystal studies works, we also include the (211), which shows an onset potential similar to the (100), but a sharper rise in activity as the potential is increased.

The onset potential of acetaldehyde (Figure 3d) and ethylene (Figure 3c) on polycrystalline Cu are substantially earlier than methane (Figure 3b), similar to what is on Cu(100) and Cu(211). This suggests that on polycrystalline Cu acetaldehyde and ethylene are both limited by C-C coupling whereas methane is generated through a separate mechanism, thus agreeing with previous findings both experimentally and theoretically [1].

The Cu(211) facet could not reach a potential more cathodic than *ca.* -0.46 V due to gas bubble formation (Figure 3e). Yet, within the scanned potential window, its ethylene (Figure 3c) and acetaldehyde (Figure 3d) formation acts similarly to polycrystalline Cu and Cu(100).

Previous *operando* EC-STM studies have revealed that both polycrystalline Cu and Cu(110) undergo surface restructuring under eCORR conditions to a more Cu(100)-rich topmost surface, while the native Cu(111) and Cu(100) surfaces do not undergo this reconstruction. This facet-dependent surface restructuring might explain the (100)-like eCORR performance of polycrystalline Cu and Cu(110) in these previous studies. [42–44] However, the previous restructuring investigation was conducted at a constant potential (-0.2 ~ -0.3 V) for 1h, while the presented eCORR data were collected within 5~6 min with LSV scans. In addition, given that the above literature show both polycrystalline Cu and (110) crystals undergo restructuring on the same time scale, and that Figure 3 only exhibits the similarity of Cu(100) with polycrystalline Cu but not with Cu(110), restructuring may not be responsible for the (100)-like polycrystalline Cu here.

Potential- and facet-dependent acetaldehyde/ethylene branching point. One of the key issues in CO_2 electrolysis is determining the branching point between ethylene and ethanol. Literature have shown that acetaldehyde is the direct precursor of ethanol, indicating the above branching happens between ethylene and acetaldehyde [7,13,21,30]. Moreover, previous findings suggested that lower overpotential tends to favor oxygenates over hydrocarbons [2,42,44–46] but with a limited precision at which potential their branching occurs. To give more insight into this issue, Figure 4 plots the ratio of acetaldehyde/ethylene on polycrystalline Cu, Cu(211), and Cu(100), which provides a detailed quantitative understanding of how these two species relate. Cu(111) and (110) facets are not plotted in Figure 4 because they do not produce acetaldehyde (Figure 3d).

In addition to potential dependency, the results also exhibit a facet dependency of the branching, especially in the -0.35 V ~ -0.45 V *vs.* RHE potential window. By plotting the data on a log scale, it is clearly seen that the acetaldehyde/ethylene ratio of polycrystalline Cu and Cu(211) decreases exponentially across the detected potential window, whereas the ratio on the (100) facet appears to be a constant ratio at lower overpotentials (> -0.45 V *vs.* RHE) and then shifts to the exponential decrease at higher overpotentials (< -0.45 V *vs.* RHE). It is worth mentioning that the signal-to-noise ratio prevents a detailed analysis and the lack of ethanol or acetate detection does limit a full analysis of the major branching. However, Figure 4 still provides a highly unique relationship regarding the potential- and facet-dependency

of acetaldehyde/ethylene branching. In coordination with other works, the presented quantitative ratio can provide valuable insights into the further understanding of the selectivity and reaction kinetics of $CO(_2)$ electrolysis products on copper.

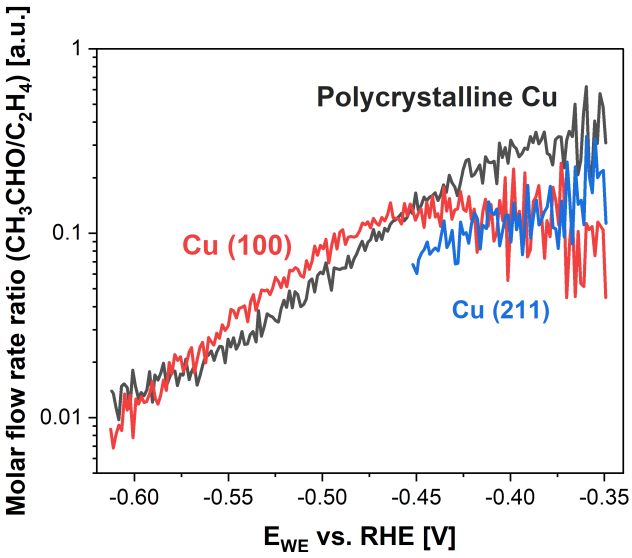

Figure 4 Molar flow rate ratio of acetaldehyde-to-ethylene on polycrystalline Cu and Cu(100) facet, respectively. Only the potential window after acetaldehyde production onset (ca. -0.35 V vs. RHE) is plotted.

In the present letter, we have first systematically demonstrated the necessity and feasibility of detecting and measuring acetaldehyde production under eCORR conditions on a real-time scale. We then presented the real-time detection of gas (hydrogen, methane, and ethylene) and volatile liquid (acetaldehyde) production on both polycrystalline and single crystal Cu electrodes during eCORR at low overpotentials (< -0.65 V). Results not only revealed a facet-dependent acetaldehyde production, but also exhibited a facet- and potential-dependent acetaldehyde/ethylene production ratio. This quantified acetaldehyde/ethylene ratio provides insightful information on the highly important bifurcation point between the pathway producing these two products in eCORR/eCO2RR. While the real-time acetaldehyde production detection on polycrystalline and single crystal Cu provides new fundamental data for the field, the importance of this data becomes greatly magnified when we relate it to ethylene production and note the exponential trend of this ratio as a function of potential.

Notes

The authors declare no competing financial interest.

Acknowledgment

B.S. and Y.Q. acknowledge European Union's Horizon 2020 research and innovation programme under grant agreement no. 85144 (SELECT-CO2), the Villum Center for the Science of Sustainable Fuels and Chemical grant 9455 (VSustain), and Capturing CO2 for simultaneous chlorine and ethanol production using sea water and sustainable electricity grant 1115-00007B (CapCO2).

Supporting Information Available

Acetaldehyde chemistry in alkaline, optimization of the MS electron energy, validation and quantification of target analytes, experimental methods and details of single crystal quality inspection of Cu(hkl) electrodes and eCORR, electrochemical setup, explanation on the unexpected high current density at 0 V *vs.* RHE.

References

(1) Nitopi, S.; Bertheussen, E.; Scott, S. B.; Liu, X.; Engstfeld, A. K.; Horch, S.; Seger, B.; Stephens, I. E. L.; Chan, K.; Hahn, C.; Nørskov, J. K.; Jaramillo, T. F.; Chorkendorff, I. Progress and Perspectives of Electrochemical CO2 Reduction on Copper in Aqueous Electrolyte. *Chem. Rev.* **2019**, *119* (12), 7610–7672. https://doi.org/10.1021/acs.chemrev.8b00705.

(2) Wang, L.; Nitopi, S. A.; Bertheussen, E.; Orazov, M.; Morales-Guio, C. G.; Liu, X.; Higgins, D. C.; Chan, K.; Nørskov, J. K.; Hahn, C.; Jaramillo, T. F. Electrochemical Carbon Monoxide Reduction on Polycrystalline Copper: Effects of Potential, Pressure, and PH on Selectivity toward Multicarbon and Oxygenated Products. *ACS Catal.* **2018**, *8* (8), 7445–7454. https://doi.org/10.1021/acscatal.8b01200.

(3) Li, J.; Wang, Z.; McCallum, C.; Xu, Y.; Li, F.; Wang, Y.; Gabardo, C. M.; Dinh, C. T.; Zhuang, T. T.; Wang, L.; Howe, J. Y.; Ren, Y.; Sargent, E. H.; Sinton, D. Constraining CO Coverage on Copper Promotes High-Efficiency Ethylene Electroproduction. *Nat. Catal.* **2019**, *2* (12), 1124–1131. https://doi.org/10.1038/s41929-019-0380-x.

(4) Bertheussen, E.; Verdaguer-Casadevall, A.; Ravasio, D.; Montoya, J. H.; Trimarco, D. B.; Roy, C.; Meier, S.; Wendland, J.; Nørskov, J. K.; Stephens, I. E. L.; Chorkendorff, I. Acetaldehyde as an Intermediate in the Electroreduction of Carbon Monoxide to Ethanol on Oxide-Derived Copper. *Angew. Chemie - Int. Ed.* **2016**, *55* (4), 1450–1454. https://doi.org/10.1002/anie.201508851.

(5) Lum, Y.; Ager, J. W. Evidence for Product-Specific Active Sites on Oxide-Derived Cu Catalysts for Electrochemical CO2 Reduction. *Nat. Catal.* **2019**, *2* (1), 86–93. https://doi.org/10.1038/s41929-018-0201-7.

(6) Jouny, M.; Luc, W.; Jiao, F. High-Rate Electroreduction of Carbon Monoxide to Multi-Carbon Products. *Nat. Catal.* **2018**, *1* (10), 748–755. https://doi.org/10.1038/s41929-018-0133-2.

(7) Ma, M.; Deng, W.; Xu, A.; Hochfilzer, D.; Qiao, Y.; Chan, K.; Chorkendorff, I.; Seger, B. Local Reaction Environment for Selective Electroreduction of Carbon Monoxide. *Energy Environ. Sci.* **2022**, *15* (6), 2470–2478. https://doi.org/10.1039/d1ee03838a.

(8) Luc, W.; Fu, X.; Shi, J.; Lv, J. J.; Jouny, M.; Ko, B. H.; Xu, Y.; Tu, Q.; Hu, X.; Wu, J.; Yue, Q.; Liu, Y.; Jiao, F.; Kang, Y. Two-Dimensional Copper Nanosheets for Electrochemical Reduction of Carbon Monoxide to Acetate. *Nat. Catal.* **2019**, *2* (5), 423–430. https://doi.org/10.1038/s41929-019-0269-8.

(9) Kuhl, K. P.; Cave, E. R.; Abram, D. N.; Jaramillo, T. F. New Insights into the Electrochemical Reduction of Carbon Dioxide on Metallic Copper Surfaces. *Energy Environ. Sci.* **2012**, *5* (5), 7050–7059. https://doi.org/10.1039/c2ee21234j.

(10) Schouten, K. J. P.; Kwon, Y.; Van Der Ham, C. J. M.; Qin, Z.; Koper, M. T. M. A New Mechanism for the Selectivity to C1 and C2 Species in the Electrochemical Reduction of Carbon Dioxide on Copper

Electrodes. *Chem. Sci.* **2011**, *2* (10), 1902–1909. https://doi.org/10.1039/c1sc00277e.

(11) Ting, L. R. L.; Piqué, O.; Lim, S. Y.; Tanhaei, M.; Calle-Vallejo, F.; Yeo, B. S. Enhancing CO2 Electroreduction to Ethanol on Copper-Silver Composites by Opening an Alternative Catalytic Pathway. *ACS Catal.* **2020**, *10* (7), 4059–4069. https://doi.org/10.1021/acscatal.9b05319.

(12) Birdja, Y. Y.; Koper, M. T. M. The Importance of Cannizzaro-Type Reactions during Electrocatalytic Reduction of Carbon Dioxide. *J. Am. Chem. Soc.* **2017**, *139* (5), 2030–2034. https://doi.org/10.1021/jacs.6b12008.

(13) Chang, X.; Malkani, A.; Yang, X.; Xu, B. Mechanistic Insights into Electroreductive C-C Coupling between CO and Acetaldehyde into Multicarbon Products. *J. Am. Chem. Soc.* **2020**, *142* (6), 2975–2983. https://doi.org/10.1021/jacs.9b11817.

(14) Ting, L. R. L.; García-Muelas, R.; Martín, A. J.; Veenstra, F. L. P.; Chen, S. T.; Peng, Y.; Per, E. Y. X.; Pablo-García, S.; López, N.; Pérez-Ramírez, J.; Yeo, B. S. Electrochemical Reduction of Carbon Dioxide to 1-Butanol on Oxide-Derived Copper. *Angew. Chemie Int. Ed.* **2020**, *59* (47), 21072–21079. https://doi.org/10.1002/anie.202008289.

(15) Birdja, Y. Y.; Pérez-Gallent, E.; Figueiredo, M. C.; Göttle, A. J.; Calle-Vallejo, F.; Koper, M. T. M. Advances and Challenges in Understanding the Electrocatalytic Conversion of Carbon Dioxide to Fuels. *Nat. Energy* **2019**, *4* (9), 732–745. https://doi.org/10.1038/s41560-019-0450-y.

(16) Furukawa, J.; Saegusa, T.; Fujii, H. Polymerization of Acetaldehyde. *Bull. Japan Pet. Inst.* **1961**, *3*, 33–38.

(17) Vogl, O. Addition Polymers of Aldehydes. *J. Polym. Sci. Part A Polym. Chem.* **2000**, *38* (13), 2293–2299. https://doi.org/10.1002/1099-0518(20000701)38:13<2293::AID-POLA10>3.0.CO;2-M.

(18) Fan, Q.; Zhang, M.; Jia, M.; Liu, S.; Qiu, J.; Sun, Z. Electrochemical CO2 Reduction to C2+ Species: Heterogeneous Electrocatalysts, Reaction Pathways, and Optimization Strategies. *Mater. Today Energy* **2018**, *10*, 280–301. https://doi.org/10.1016/j.mtener.2018.10.003.

(19) Delmo, E. P.; Wang, Y.; Zhu, S.; Li, T.; Wang, Y.; Jang, J.; Zhao, Q.; Roxas, A. P.; Nambafu, G. S.; Luo, Z.; Weng, L. T.; Shao, M. The Role of Glyoxal as an Intermediate in the Electrochemical CO2 Reduction Reaction on Copper. *J. Phys. Chem. C* **2023**, *127* (9), 4496–4510. https://doi.org/10.1021/acs.jpcc.3c00589.

(20) Ma, M.; Clark, E. L.; Therkildsen, K. T.; Dalsgaard, S.; Chorkendorff, I.; Seger, B. Insights into the Carbon Balance for CO2 Electroreduction on Cu Using Gas Diffusion Electrode Reactor Designs. *Energy Environ. Sci.* **2020**, *13* (3), 977–985. https://doi.org/10.1039/d0ee00047g.

(21) Peng, H. J.; Tang, M. T.; Halldin Stenlid, J.; Liu, X.; Abild-Pedersen, F. Trends in Oxygenate/Hydrocarbon Selectivity for Electrochemical CO(2) Reduction to C2 Products. *Nat. Commun.* **2022**, *13* (1), 1–11. https://doi.org/10.1038/s41467-022-29140-8.

(22) Trimarco, D. B.; Scott, S. B.; Thilsted, A. H.; Pan, J. Y.; Pedersen, T.; Hansen, O.; Chorkendorff, I.; Vesborg, P. C. K. Enabling Real-Time Detection of Electrochemical Desorption Phenomena with Sub-Monolayer Sensitivity. *Electrochim. Acta* **2018**, *268*, 520–530. https://doi.org/10.1016/j.electacta.2018.02.060.

(23) Linstrom, P. J.; Mallard, W. G. The NIST Chemistry WebBook: A Chemical Data Resource on the Internet. *J. Chem. Eng. Data* **2001**, *46* (5), 1059–1063. https://doi.org/10.1021/je000236i.

(24) Kempler, P. A.; Nielander, A. C. Reliable Reporting of Faradaic Ef Fi Ciencies for Electrocatalysis Research. https://doi.org/10.1038/s41467-023-36880-8.

(25) Christophe, J.; Doneux, T.; Buess-Herman, C. Electroreduction of Carbon Dioxide on Copper-Based Electrodes: Activity of Copper Single Crystals and Copper-Gold Alloys. *Electrocatalysis* **2012**, *3* (2), 139–146. https://doi.org/10.1007/s12678-012-0095-0.

(26) Gao, S. T.; Xiang, S. Q.; Shi, J. L.; Zhang, W.; Zhao, L. Bin. Theoretical Understanding of the Electrochemical Reaction Barrier: A Kinetic Study of CO2 Reduction Reaction on Copper Electrodes. *Phys. Chem. Chem. Phys.* **2020**, *22* (17), 9607–9615. https://doi.org/10.1039/c9cp06824d.

(27) Zhong, D.; Zhao, Z. J.; Zhao, Q.; Cheng, D.; Liu, B.; Zhang, G.; Deng, W.; Dong, H.; Zhang, L.; Li, J.; Li, J.; Gong, J. Coupling of Cu(100) and (110) Facets Promotes Carbon Dioxide Conversion to Hydrocarbons and Alcohols. *Angew. Chemie - Int. Ed.* **2021**, *60* (9), 4879–4885. https://doi.org/10.1002/anie.202015159.

(28) Schouten, K. J. P.; Pérez Gallent, E.; Koper, M. T. M. Structure Sensitivity of the Electrochemical Reduction of Carbon Monoxide on Copper Single Crystals. *ACS Catal.* **2013**, *3* (6), 1292–1295. https://doi.org/10.1021/cs4002404.

(29) Li, H.; Li, Y.; Koper, M. T. M.; Calle-Vallejo, F. Bond-Making and Breaking between Carbon, Nitrogen, and Oxygen in Electrocatalysis. *J. Am. Chem. Soc.* **2014**, *136* (44), 15694–15701. https://doi.org/10.1021/ja508649p.

(30) Cheng, D.; Zhao, Z. J.; Zhang, G.; Yang, P.; Li, L.; Gao, H.; Liu, S.; Chang, X.; Chen, S.; Wang, T.; Ozin, G. A.; Liu, Z.; Gong, J. The Nature of Active Sites for Carbon Dioxide Electroreduction over Oxide-Derived Copper Catalysts. *Nat. Commun.* **2021**, *12* (1), 1–8. https://doi.org/10.1038/s41467-020-20615-0.

(31) Hori, Y.; Wakebe, H.; Tsukamoto, T.; Koga, O. Adsorption of CO Accompanied with Simultaneous Charge Transfer on Copper Single Crystal Electrodes Related with Electrochemical Reduction of CO2 to Hydrocarbons. *Surf. Sci.* **1995**, *335* (C), 258–263. https://doi.org/10.1016/0039-6028(95)00441-6.

(32) Montoya, J. H.; Shi, C.; Chan, K.; Nørskov, J. K. Theoretical Insights into a CO Dimerization Mechanism in CO2 Electroreduction. *J. Phys. Chem. Lett.* **2015**, *6* (11), 2032–2037. https://doi.org/10.1021/acs.jpclett.5b00722.

(33) Schouten, K. J. P.; Qin, Z.; Gallent, E. P.; Koper, M. T. M. Two Pathways for the Formation of Ethylene in CO Reduction on Single-Crystal Copper Electrodes. *J. Am. Chem. Soc.* **2012**, *134* (24), 9864–9867. https://doi.org/10.1021/ja302668n.

(34) Garza, A. J.; Bell, A. T.; Head-Gordon, M. Mechanism of CO2 Reduction at Copper Surfaces: Pathways to C2 Products. *ACS Catal.* **2018**, *8* (2), 1490–1499. https://doi.org/10.1021/acscatal.7b03477.

(35) Hori, Y.; Takahashi, I.; Koga, O.; Hoshi, N. Selective Formation of C2 Compounds from Electrochemical Reduction of CO2 at a Series of Copper Single Crystal Electrodes. *J. Phys. Chem. B* **2002**, *106* (1), 15–17. https://doi.org/10.1021/jp013478d.

(36) Takahashi, I.; Koga, O.; Hoshi, N.; Hori, Y. Electrochemical Reduction of CO2 at Copper Single Crystal Cu(S)-[n(111) × (111)] and Cu(S)-[n(110) × (100)] Electrodes. *J. Electroanal. Chem.* **2002**, *533* (1–2), 135–143. https://doi.org/10.1016/S0022-0728(02)01081-1.

(37) Hori, Y.; Takahashi, I.; Koga, O.; Hoshi, N. Electrochemical Reduction of Carbon Dioxide at Various Series of Copper Single Crystal Electrodes. *J. Mol. Catal. A Chem.* **2003**, *199* (1–2), 39–47. https://doi.org/10.1016/S1381-1169(03)00016-5.

(38) Pérez-Gallent, E.; Marcandalli, G.; Figueiredo, M. C.; Calle-Vallejo, F.; Koper, M. T. M. Structure- and Potential-Dependent Cation Effects on CO Reduction at Copper Single-Crystal Electrodes. *J. Am. Chem. Soc.* **2017**, *139* (45), 16412–16419. https://doi.org/10.1021/jacs.7b10142.

(39) Roberts, F. S.; Kuhl, K. P.; Nilsson, A. High Selectivity for Ethylene from Carbon Dioxide Reduction over Copper Nanocube Electrocatalysts. *Angew. Chemie - Int. Ed.* **2015**, *54* (17), 5179–5182. https://doi.org/10.1002/anie.201412214.

(40) Bagger, A.; Ju, W.; Varela, A. S.; Strasser, P.; Rossmeisl, J. Electrochemical CO2 Reduction: Classifying Cu Facets. *ACS Catal.* **2019**, *9* (9), 7894–7899. https://doi.org/10.1021/acscatal.9b01899.

(41) Kastlunger, G.; Wang, L.; Govindarajan, N.; Heenen, H. H.; Ringe, S.; Jaramillo, T.; Hahn, C.; Chan, K. Using PH Dependence to Understand Mechanisms in Electrochemical CO Reduction. *ACS Catal.* **2022**, *12* (8), 4344–4357. https://doi.org/10.1021/acscatal.1c05520.

(42) Kim, Y. G.; Javier, A.; Baricuatro, J. H.; Soriaga, M. P. Regulating the Product Distribution of CO Reduction by the Atomic-Level Structural Modification of the Cu Electrode Surface. *Electrocatalysis* **2016**, *7* (5), 391–399. https://doi.org/10.1007/s12678-016-0314-1.

(43) Kim, Y. G.; Javier, A.; Baricuatro, J. H.; Torelli, D.; Cummins, K. D.; Tsang, C. F.; Hemminger, J. C.; Soriaga, M. P. Surface Reconstruction of Pure-Cu Single-Crystal Electrodes under CO-Reduction Potentials in Alkaline Solutions: A Study by Seriatim ECSTM-DEMS. *J. Electroanal. Chem.* **2016**, *780*, 290–295. https://doi.org/10.1016/j.jelechem.2016.09.029.

(44) Kwon, S.; Kim, Y. G.; Baricuatro, J. H.; Goddard, W. A. Dramatic Change in the Step Edges of the Cu(100) Electrocatalyst upon Exposure to CO: Operando Observations by Electrochemical STM and Explanation Using Quantum Mechanical Calculations. *ACS Catal.* **2021**, *11* (19), 12068–12074. https://doi.org/10.1021/acscatal.1c02844.

(45) Baricuatro, J. H.; Kim, Y. G.; Tsang, C. F.; Javier, A. C.; Cummins, K. D.; Hemminger, J. C. Selective Conversion of CO into Ethanol on Cu(511) Surface Reconstructed from Cu(Pc): Operando Studies by Electrochemical Scanning Tunneling Microscopy, Mass Spectrometry, Quartz Crystal Nanobalance, and Infrared Spectroscopy. *J. Electroanal. Chem.* **2020**, *857*, 113704. https://doi.org/10.1016/j.jelechem.2019.113704.

(46) Ruiz-López, E.; Gandara-Loe, J.; Baena-Moreno, F.; Reina, T. R.; Odriozola, J. A. Electrocatalytic CO2 Conversion to C2 Products: Catalysts Design, Market Perspectives and Techno-Economic Aspects. *Renew. Sustain. Energy Rev.* **2022**, *161* (February). https://doi.org/10.1016/j.rser.2022.112329.